

Supplementary Material

Optimisation of iron oxide nanoparticles for agglomeration and blockage in aqueous flow systems

Lila M. Landowski,^[a] Karen L. Livesey,^[b] Olivier Bibari,^[a] Allanna M. Russell,^[a] Madeleine R. Taylor,^[c]
Curtis C. Ho,^[c] David W. Howells^[a] and Rebecca O. Fuller,^{[c]*}

^[a] Tasmanian School of Medicine, University of Tasmania, Hobart, Tas. 7005, Australia

^[b] School of Mathematical and Physical Sciences, The University of Newcastle, Callaghan, NSW 2308, Australia.

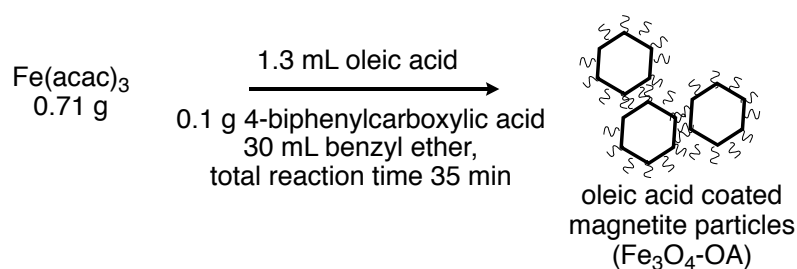
^[c] School of Natural Sciences-Chemistry, University of Tasmania, Hobart, Tas. 7005, Australia.

*Corresponding author. Email: rebecca.fuller@utas.edu.au

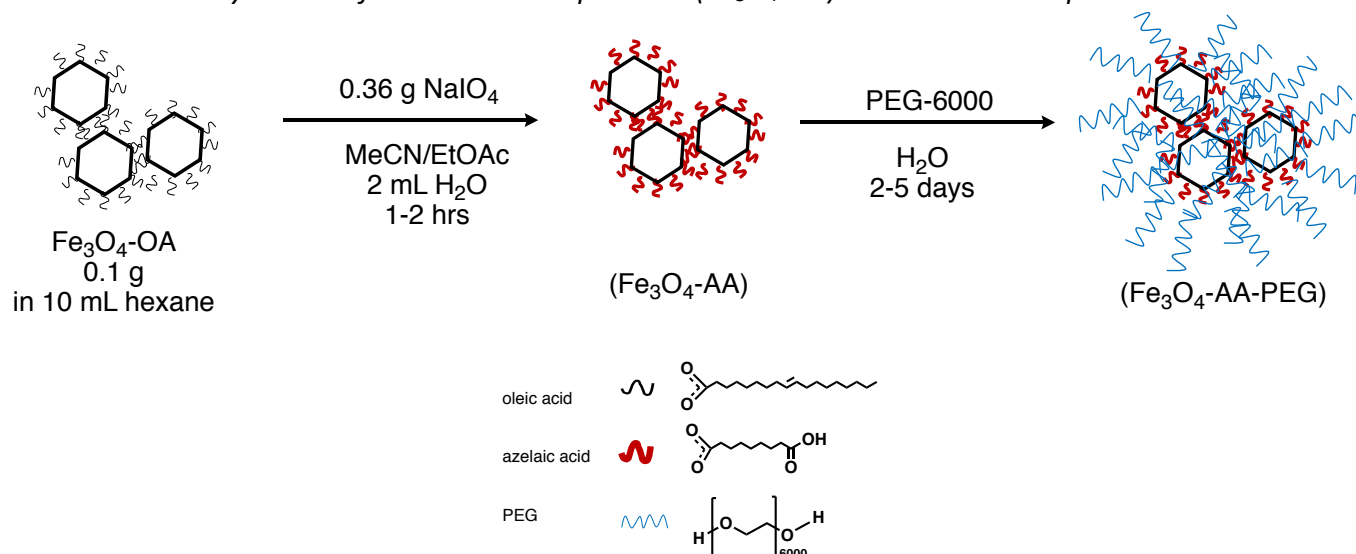
Table of Contents

I.	Synthesis of Iron Oxide Particles	S-1
II.	Characterisation of iron oxide particles	S-4
III.	Flow experiments	S-10

I. Synthesis of Iron Oxide Particles



Scheme S1: Synthesis of iron oxide nanoparticles ($\text{Fe}_3\text{O}_4\text{-OA}$) detailed in the experimental section.



Scheme 2: Modification of $\text{Fe}_3\text{O}_4\text{-OA}$ surface. Oxidative cleavage results in a hydrophilic system through the formation of azelaic acid coated particles ($\text{Fe}_3\text{O}_4\text{-AA}$); Further stability in water is achieved through the addition of PEG ($\text{Fe}_3\text{O}_4\text{-AA-PEG}$) to the surface.

Figure S1a: Reaction set up using a gas manifold where (a) illustrates a simple degassing procedure; (b) foiling/stoppering of flask prior to reaction; (c) end of reaction, foil has been removed for clarity; (d) flasks are totally removed from mantles for cooling.



Figure S1b: (left) A demonstration of how the magnet is removed, using a second externally placed magnet. As the magnet is sitting in a position similar to the one indicated above, a solution of toluene/hexane is squirted onto the magnet, to remove nanoparticles that adhere to the magnet. (right) Typical example of the appearance of nanoparticles after centrifugation following their second wash. The supernatant will be a straw yellow colour.

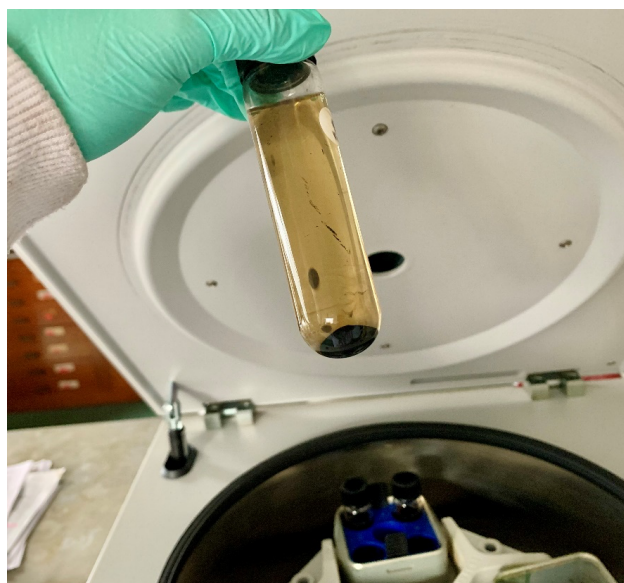
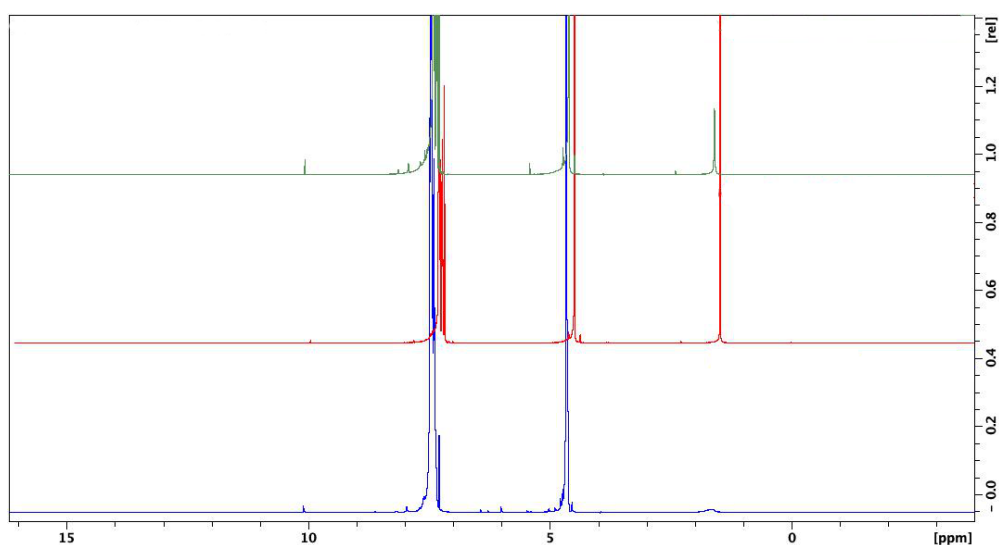


Table S1: GC-MS data of benzyl ether

benzyl ether	Peak	Retention time	Relative Abundance %	ID	CAS
Naturally aged 16 months (Aldrich 108014-1kg Lot#MKCC9034)	A	2.59	1.98	benzaldehyde	000100-52-7
	B	3.18	0.66	benzyl alcohol	000100-51-6
	C	11.12	100	benzyl ether	000103-50-4
	D	12.46	0.83	benzyl benzoate	000120-51-4
Pristine (Aldrich 108014- 1kg Lot#SHBL6366)	A	2.59	0.42	benzaldehyde	000100-52-7
	B	3.19	0.07	benzyl alcohol	000100-51-6
	C	11.12	100	benzyl ether	000103-50-4
	D	12.47	0.10	benzyl benzoate	000120-51-4
Entry 11 (Table 2) pristine (Aldrich 108014- 1kg Lot#SHBL6366) with additives	A	2.59	3.96	benzaldehyde	000100-52-7
	B	3.19	0.62	benzyl alcohol	000100-51-6
	C	11.12	100	benzyl ether	000103-50-4
	D	12.47	1.02	benzyl benzoate	000120-51-4
Artificially aged (Aldrich 108014-1kg Lot#SHBL6366) after 1hr compressed air	A	2.59	0.53	benzaldehyde	000100-52-7
	B	3.19	0.08	benzyl alcohol	000100-51-6
	C	11.17	100	benzyl ether	000103-50-4
	D	12.49	0.08	benzyl benzoate	000120-51-4
Artificially aged (Aldrich 108014-1kg Lot#SHBL6366) after 7hr compressed air	A	2.59	0.47	benzaldehyde	000100-52-7
	B	3.19	0.08	benzyl alcohol	000100-51-6
	C	11.12	100	benzyl ether	000103-50-4
	D	12.46	0.23	benzyl benzoate	000120-51-4
Artificially aged (Aldrich 108014-1kg Lot#SHBL6366) after 24 hr compressed air	A	2.59	0.52	benzaldehyde	000100-52-7
	B	3.18	0.10	benzyl alcohol	000100-51-6
	C	11.12	100	benzyl ether	000103-50-4
	D	12.46	0.38	benzyl benzoate	000120-51-4
Artificially aged (Aldrich 108014-1kg Lot#SHBL6366) after 96 hr compressed air	A	2.59	1.91	benzaldehyde	000100-52-7
	B	3.18	0.40	benzyl alcohol	000100-51-6
	C	11.12	100	benzyl ether	000103-50-4
	D	12.46	1.42	benzyl benzoate	000120-51-4
Artificially aged (Aldrich 108014-1kg Lot#SHBL6366) after 1 week compressed air	A	2.59	3.23	benzaldehyde	000100-52-7
	B	3.19	0.62	benzyl alcohol	000100-51-6
	C	11.11	100	benzyl ether	000103-50-4
	D	12.44	2.19	benzyl benzoate	000120-51-4

Figure S2: ^1H NMR for benzyl ether aged 16 months (blue), pristine benzyl ether (red), pristine benzyl ether with additives entry 11 (green).

II. Characterisation of Iron Oxide Particles

Figure S3: Characterisation of **1b**; (a) Bright Field TEM image; (b) XRD pattern; (c) Raman Spectrum.

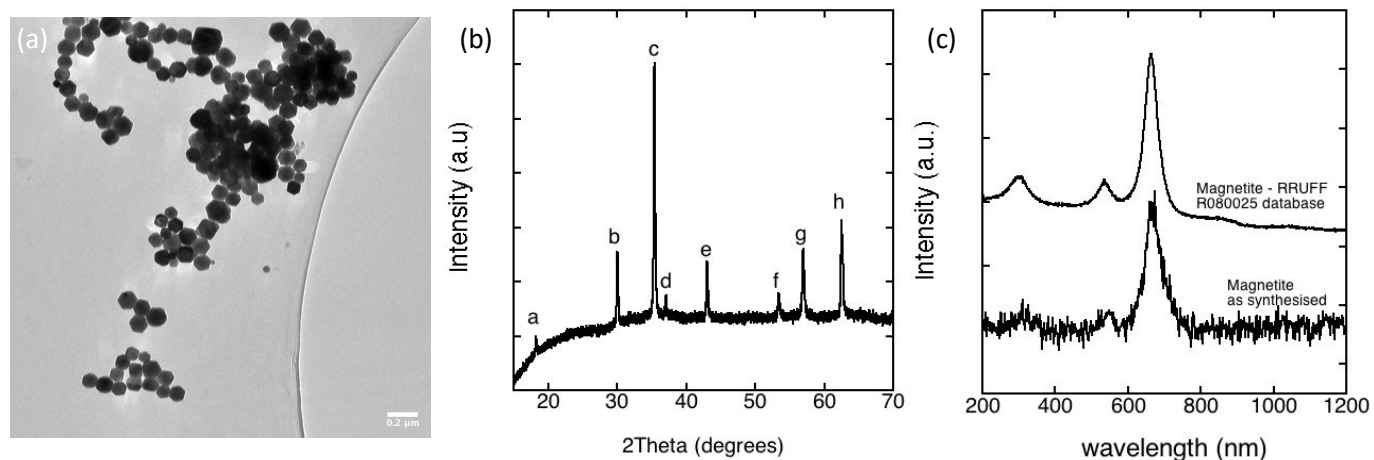
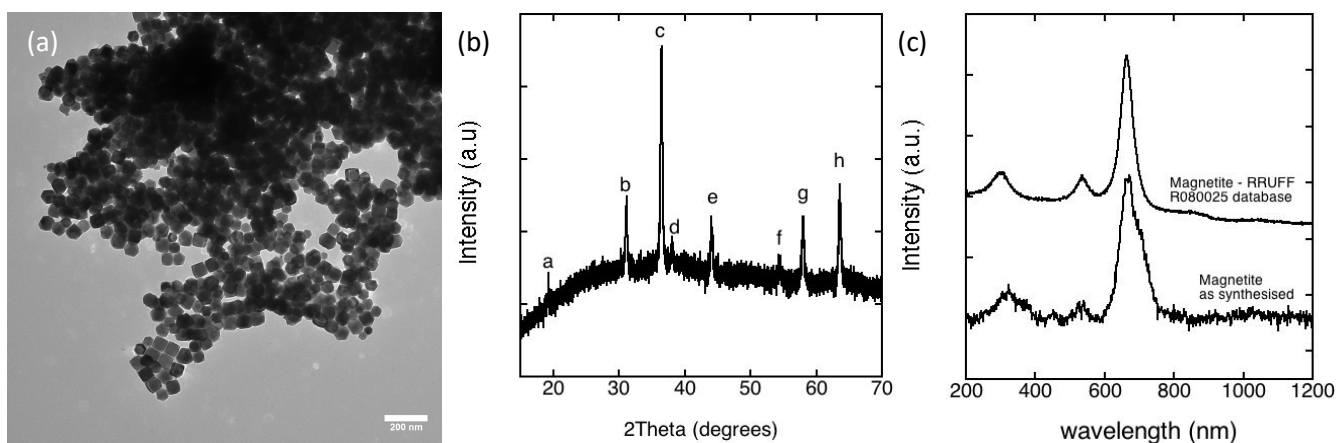


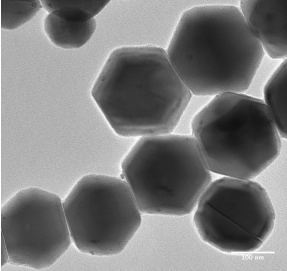
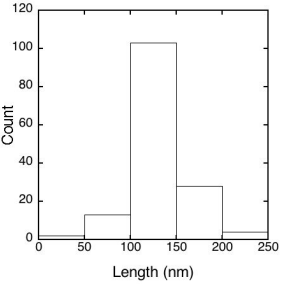
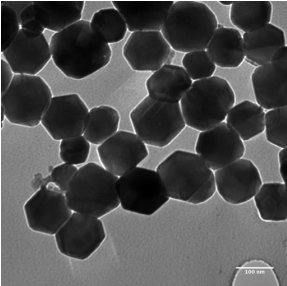
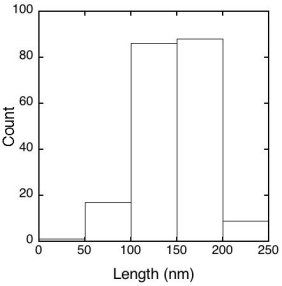
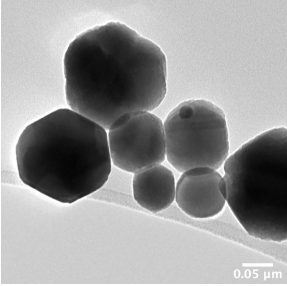
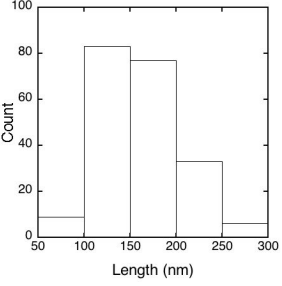
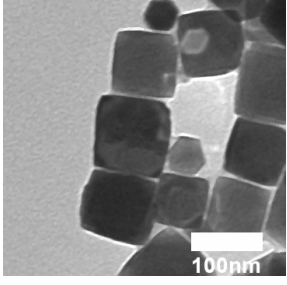
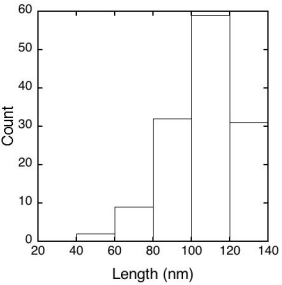
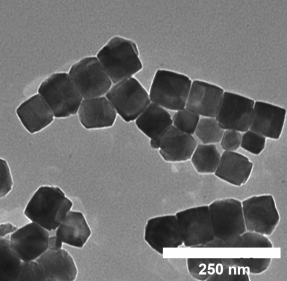
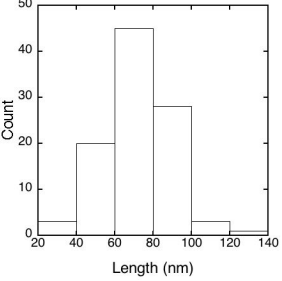
Table S2: Comparison of *d*-spacings for **1b** from powder XRD for **1b** with JCPDS cards #75-0033 and #39-1346.

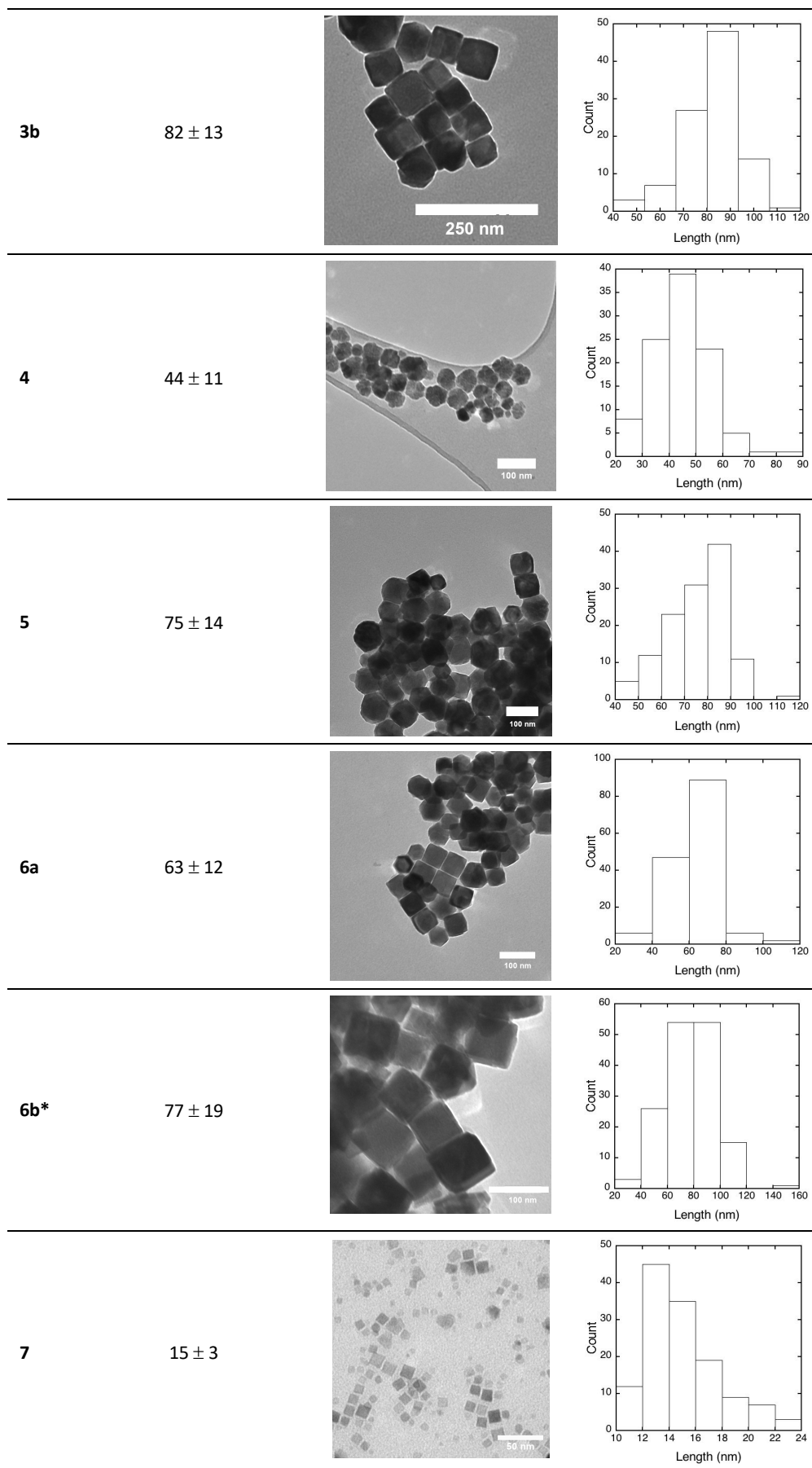
entry	hkl	Measured XRD <i>d</i> -spacings (nm)	Fe ₃ O ₄ (JCPDS 75-0033) (nm)	γ-Fe ₂ O ₃ (JCPDS 39-1346) (nm)
a	111	0.486	0.484	0.482
b	220	0.297	0.296	0.295
c	311	0.253	0.253	0.252
d	222	0.242	0.242	0.241
e	400	0.210	0.210	0.209
f	422	0.172	0.171	0.170
g	511	0.162	0.161	0.161
h	440	0.149	0.148	0.148

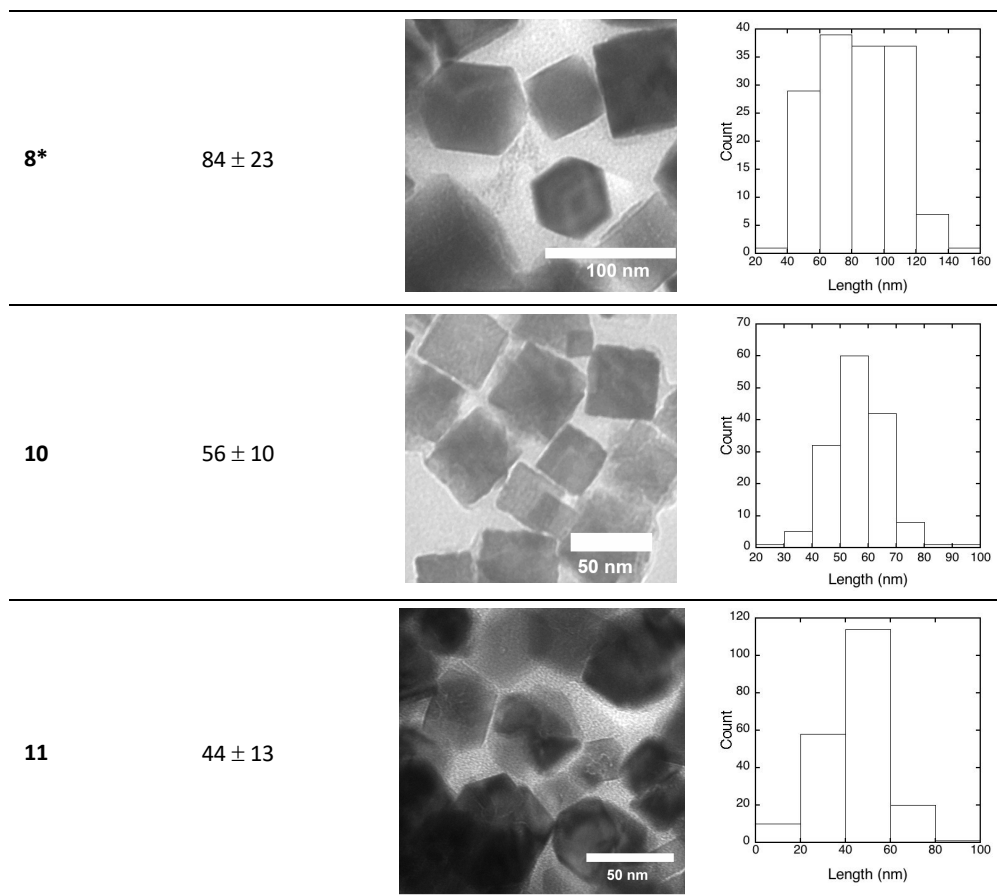
Figure S4: Characterisation of **6a**; (a) Bright Field TEM image; (b) XRD pattern; (c) Raman Spectrum.Table S3: Comparison of *d*-spacings for **6a** from powder XRD for **1a** with JCPDS cards #75-0033 and #39-1346.

entry	hkl	Measured XRD <i>d</i> -spacings (nm)	Fe ₃ O ₄ (JCPDS 75-0033) (nm)	γ-Fe ₂ O ₃ (JCPDS 39-1346) (nm)
a	111	0.481	0.484	0.482
b	220	0.294	0.296	0.295
c	311	0.251	0.253	0.252
d	222	-	0.242	0.241
e	400	0.201	0.210	0.209
f	422	0.171	0.171	0.170
g	511	0.161	0.161	0.161
h	440	0.148	0.148	0.148

Table S4: A representative bright field TEM image of as-synthesised (Table 1 and 2) iron oxide nanocrystals. Histogram of the size distribution obtained from measurements is included.

entry	Diameter of particles (nm)	TEM	Size Distribution
1a	131 ± 30		
1b	146 ± 36		
1c	158 ± 42		
2	107 ± 18		
3a	72 ± 17		





*Four repeat reactions were performed; reactions were combined prior to work up;

Figure S5: FTIR(ATR) used to observe the oxidative cleavage of magnetite particles from **6a**. The upper trace contains as-synthesised Fe_3O_4 -OA with the lower trace for particles after oxidative cleavage (Fe_3O_4 -AA).

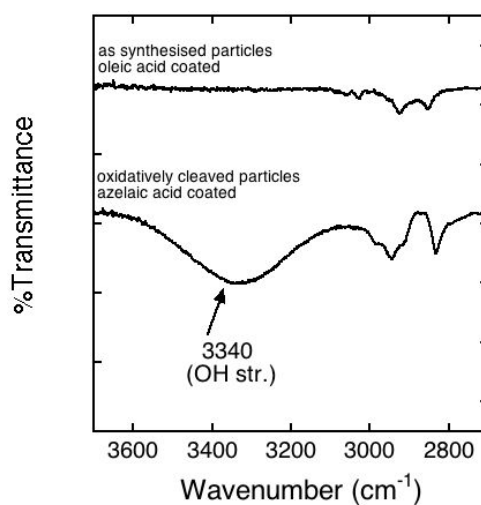
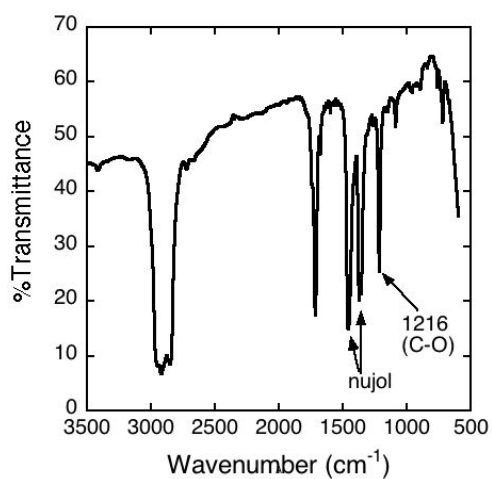


Figure S6: FTIR(nujol) of Fe_3O_4 -AA-PEG (**5**) and PEG, a strong C-O str is evident in the particles.



III. Flow experiments

Figure S7: (left) a schematic representation and (right) image of the in-house flow system used in the experiments.

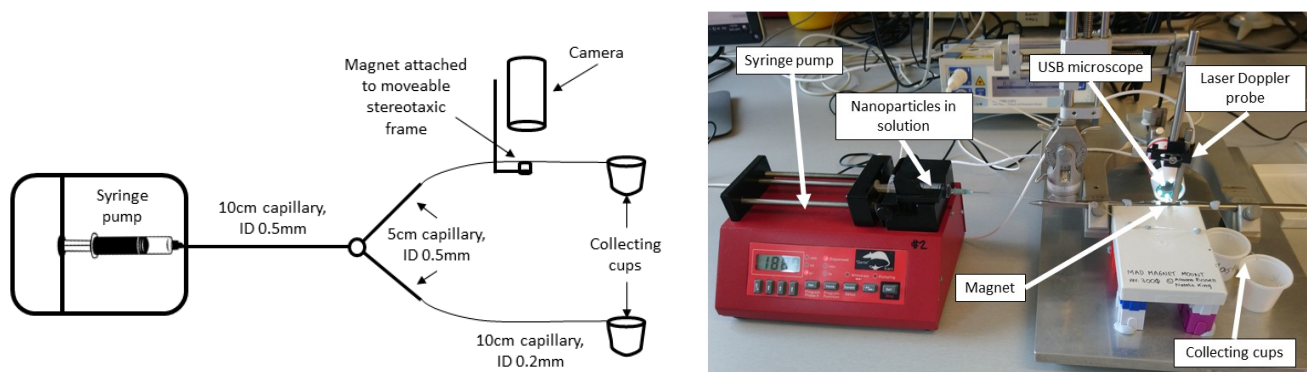


Figure S8: Flow experiments for **1b** ($\text{Fe}_3\text{O}_4\text{-AA-PEG}$). Distance between the magnet and capillary tubing = 0 mm.

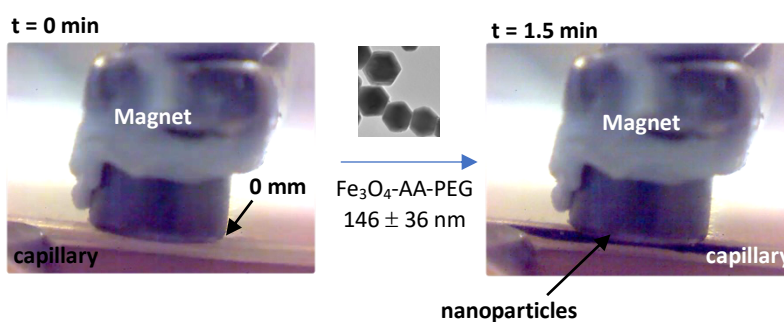


Figure S9: Flow experiments for **5** ($\text{Fe}_3\text{O}_4\text{-AA-PEG}$). Distance between the magnet and capillary tubing = 0 mm.

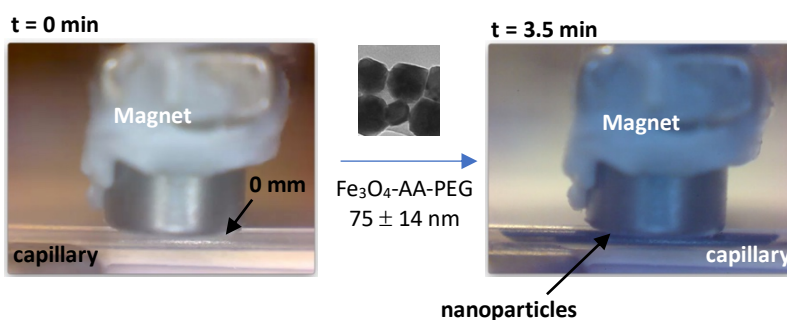


Figure S10: Flow experiments for **5** (Fe_3O_4 -AA-PEG). Distance between the magnet and capillary tubing = 1 mm.

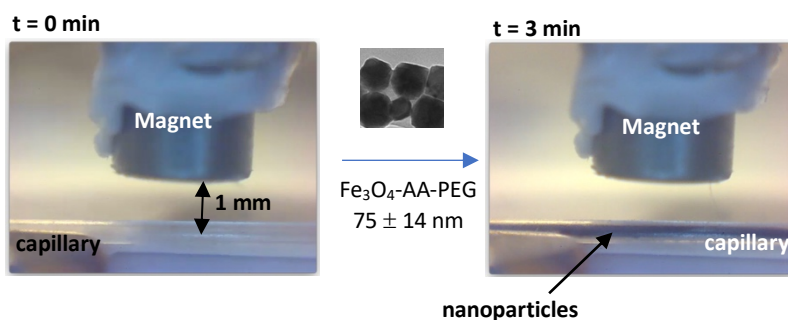


Figure S11: Flow experiments for **3b** (Fe_3O_4 -AA-PEG). Distance between the magnet and capillary tubing = 1 mm.

